STRUCTURAL BIOLOGY COMMUNICATIONS

ISSN 2053-230X

Effects of the T337M and G391V disease-related variants on human phosphoglucomutase 1: structural disruptions large and small

Kyle M. Stiers, Luckio F. Owuocha and Lesa J. Beamer*

Biochemistry Department, University of Missouri, Columbia, MO 65211, USA. *Correspondence e-mail: beamerl@missouri.edu

Received 17 February 2022
Accepted 19 April 2022

Edited by R. Sankaranarayanan, Centre for Cellular and Molecular Biology, Hyderabad, India

Keywords: missense variants; enzymes; inherited diseases; X-ray crystallography; congenital disorders of glycosylation; structural perturbation; human phosphoglucomutase 1.

PDB references: phosphoglucomutase 1, G391V variant, 7s77; T337M variant, 7s0w

Supporting information: this article has supporting information at journals.iucr.org/f

Phosphoglucomutase 1 (PGM1) plays a central role in glucose homeostasis in human cells. Missense variants of this enzyme cause an inborn error of metabolism, which is categorized as a congenital disorder of glycosylation. Here, two disease-related variants of PGM1, T337M and G391V, which are both located in domain 3 of the four-domain protein, were characterized via X-ray crystallography and biochemical assays. The studies show multiple impacts resulting from these dysfunctional variants, including both short- and long-range structural perturbations. In the T337M variant these are limited to a small shift in an active-site loop, consistent with reduced enzyme activity. In contrast, the G391V variant produces a cascade of structural perturbations, including displacement of both the catalytic phosphoserine and metal-binding loops. This work reinforces several themes that were found in prior studies of dysfunctional PGM1 variants, including increased structural flexibility and the outsized impacts of mutations affecting interdomain interfaces. The molecular mechanisms of PGM1 variants have implications for newly described inherited disorders of related enzymes.

1. Introduction

The enzyme phosphoglucomutase 1 (PGM1) is responsible for the maintenance of glucose homeostasis in most human tissues, where it catalyzes the reversible conversion of glucose 1-phosphate and glucose 6-phosphate (Quick *et al.*, 1974). PGM1 also plays a role in protein N-linked glycosylation, a common post-translational modification that is necessary for the correct function of many proteins (Schjoldager *et al.*, 2020). Various mutations reducing the activity of PGM1 have been identified that cause a congenital disorder of glycosylation [PGM1-CDG; Online Mendelian Inheritance in Man (OMIM) database entry 614921] with additional features of a glycogen-storage disease (Pérez *et al.*, 2013; Timal *et al.*, 2012; Tegtmeyer *et al.*, 2014; Stojkovic *et al.*, 2009; Ondruskova *et al.*, 2014). Affected patients show multiple phenotypes, including hepatopathy, hypoglycemia, myopathy, developmental malformations, coagulopathy, endocrine disorders, intellectual disability and both dilated and restrictive cardiomyopathies (Tegtmeyer *et al.*, 2014; Wong *et al.*, 2015; Morava *et al.*, 2015; Altassan *et al.*, 2021; Donoghue *et al.*, 2021). Dietary supplementation with oral D-galactose has been shown to benefit PGM1-CDG patients through a rewiring of sugar metabolism (Radenkovic *et al.*, 2019), although not all disease symptoms resolve with this treatment (Nolting *et al.*, 2017). While considered a rare disease, novel variants associated with PGM1-CDG continue to be identified (Donoghue *et al.*, 2021),

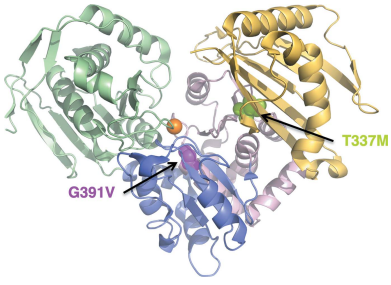

and mild phenotypes in some patients may go undiagnosed, resulting in under-reporting of the condition.

To date, approximately 25 missense variants in the 562-residue protein PGM1 have been confirmed as causing PGM1-CDG (Tegtmeyer *et al.*, 2014; Küçükçongar *et al.*, 2015; Zeevaert *et al.*, 2016; Wong *et al.*, 2015; Donoghue *et al.*, 2021). Previous biochemical and structural studies of PGM1 variants have been conducted by our laboratory, revealing a range of effects on enzyme function and structure (for a review, see Beamer, 2021). For example, an initial study found multiple missense variants that affect protein folding and solubility (Lee *et al.*, 2014). In other cases, the variant proteins proved to be quite well behaved in solution and were amenable to detailed structural characterization. More than ten crystal structures have been determined of WT PGM1 and mutant proteins, demonstrating both local and global structural perturbations (Stiers *et al.*, 2016; Stiers, Graham *et al.*, 2017), effects on protein dynamics (Stiers & Beamer, 2018*a*) and changes in stability (Stiers *et al.*, 2020). While some common themes have emerged from these studies, it remains difficult to predict the biochemical and structural impacts on PGM1 based solely on the genotype of the variant.

Here, we report structural and biochemical studies of two additional PGM1 missense variants, T337M and G391V, involving two highly conserved residues located in domain 3 of the multi-domain enzyme (Lee *et al.*, 2014; Ding *et al.*, 2018; Ondruskova *et al.*, 2014; Wong *et al.*, 2015). Biochemical data reveal generally similar effects of the two variants on protein stability and enzyme activity. In contrast, crystal structures show that the structural impacts vary significantly in both the extent and nature of the perturbation. The T337M and G391V variants belong to a subset of disease-related mutations located near interdomain interfaces of PGM1, with significantly detrimental effects on enzyme function.

2. Materials and methods

2.1. Protein expression, purification and crystallization

The T337M and G391V variants were constructed using the QuikChange kit (Agilent) and were verified by automated DNA sequencing. These two missense variants, along with the previously characterized G291R variant, were expressed recombinantly (Table 1) and purified to homogeneity via an N-terminal His_6 affinity tag, as described previously (Lee *et al.*, 2014). The purified proteins were dialyzed and concentrated as described in Table 2. If not used immediately, samples were flash-frozen in liquid nitrogen and stored at −80°C. The T337M variant crystallized under similar conditions to wild-type (WT) PGM1 (Table 2). The G391V variant crystallized in condition 2-33 of the Morpheus crystal screen (Molecular Dimensions) as detailed in Table 2.

2.2. Assessment of protein phosphorylation by mass spectrometry

The phosphorylation state of the active-site phosphoserine (Ser117) in the intact protein was analyzed for both the T337M and G391V variants before and after treatment with the activator glucose 1,6-bisphosphate (G16P) using electrospray ionization mass spectrometry (Table 1; Supplementary Fig. S1). Protein samples at concentrations between 75 and 150 µ*M* in 50 m*M* 3-(*N*-morpholino)propanesulfonic acid (MOPS) pH 7.4, 1 m*M* $MgCl_2$ were incubated with a sixfold molar excess of glucose 1,6-bisphosphate for 16 h at 4°C. For mass-spectrometric analyses, protein samples at 1 pmol μl^{-1} in 1% formic acid were analyzed by NanoLC Nanospray QTOF (Agilent 6520) in positive-ion mode using a Zorbax C8 trap column. Data were examined using the *Qual* software provided with the instrument. The mass error between samples is 0.11 Da (2.1 p.p.m.) and the quantification error is 2%. The percent phosphorylation was calculated by normalizing the sum of the dephosphorylated and phosphorylated peak heights to 1.0.

Table 1
Macromolecule-production information.

Source organism	*Homo sapiens*
Expression vector	pET-14b
Expression host	*E. coli* BL21(DE3) cells
Complete amino-acid sequence of the construct produced†	MHHHHHHSSGVDLGTENLYFQSNMVKIVTV KTQAYQDQKPGTSGLRKRVKVFQSSANY AENFIQSIISTVEPAQRQEATLVVGGDG RFYMKEAIQLIARIAAANGIGRLVIGQN GILSTPAVSCIIRKIKAIGGIILTASHN PGGPNGDFGIKFNISNGGPAPEAITDKI FQISKTIEEYAVCPDLKVDLGVLGKQQF DLENKFKPFTVEIVDSVEAYATMLRSIF DFSALKELLSGPNRLKIRIDAMHGVVGP YVKKILCEELGAPANSAVNCVPLEDFGG HHPDPNLTYAADLVETMKSGEHDFGAAF DGDGDRNMILGKHGFFVNPSDSVAVIAA NIFSIPYFQQTGVRGFARSMP**T**SGALDR VASATKIALYETPTGWKFFGNLMDASKL SLCGEESFGTGSDHIREKD**G**LWAVLAWL SILATRKQSVEDILKDHWQKYGRNFFTR YDYEEVEAEGANKMMKDLEALMFDRSFV GKQFSANDKVYTVEKADNFEYSDPVDGS ISRNQGLRLIFTDGSRIVFRLSGTGSAG ATIRLYIDSYEKDVAKINQDPQVMLAPL ISIALKVSQLQERTGRTAPTVIT

† The positions of the disease-related mutations are shown in bold and are underlined.

2.3. Kinetic characterization

The phosphoglucomutase activity of the G391V missense mutant was assessed by coupling the formation of glucose 6-phosphate from glucose 1-phosphate to NADH formation via glucose 6-phosphate dehydrogenase (G6PDH). *Leuconostoc mesenteroides* G6PDH, α-D-glucose 1-phosphate and glucose 1,6-bisphosphate were obtained from Sigma. Reactions were conducted at 25°C in 50 m*M* MOPS pH 7.4 with 1 m*M* dithiothreitol, 1.5 m*M* $MgSO_4$ and 0.9 m*M* NAD^+. G16P was present at 1.0 µ*M* and the substrate (α-D-glucose 1-phosphate) was present at 200 µ*M*. Assays of the variant were performed in parallel with a control (WT enzyme at 4.5 n*M*) and were monitored for at least 1 h. Enzyme concentrations of G391V at 1×, 10× and 100× the WT control were assessed. While activity was detectable at 100×, the slow

Table 2
Crystallization.

	T337M	G391V
PDB code	7s0w	7s77
Method	Hanging-drop vapor diffusion	Hanging-drop vapor diffusion
Plate type	VDX plate	VDX plate
Temperature (K)	293	293
Protein concentration (mg ml^{-1})	12	10
Buffer composition of protein solution	50 m*M* MOPS pH 7.4, 1 m*M* $MgCl_2$	50 m*M* MOPS pH 7.4, 1 m*M* $MgCl_2$
Composition of reservoir solution	1.8 *M* ammonium sulfate, 0.1 *M* MES pH 6.5, 0.01 *M* cobalt chloride	0.1 *M* of a carboxylic acid mixture (0.2 *M* sodium formate, 0.2 *M* ammonium acetate, 0.2 *M* sodium citrate tribasic dihydrate, 0.2 *M* sodium potassium tartrate tetrahydrate, 0.2 *M* sodium oxamate), 0.1 *M* of a buffer system at pH 8.5 (Tris base and Bicine) and a 30%(*v*/*v*) precipitant mix [40%(*v*/*v*) PEG 500 MME and 20%(*w*/*v*) PEG 20 000]
Volume and ratio of drop	4 µl (1:1)	5 µl (1:4)
Volume of reservoir (ml)	500	500

Table 3
Data collection and processing.

Values in parentheses are for the outer shell.

	T337M	G391V
PDB code	7s0w	7s77
Diffraction source	4.2.2, ALS	19-ID, APS
Wavelength (Å)	1.00003	0.999990
Temperature (K)	100	100
Detector	Taurus-1 CMOS	PILATUS
Crystal-to-detector distance (mm)	300.7	353.1
Rotation range per image (°)	0.2	0.2
Total rotation range (°)	180	180
Exposure time per image (s)	0.3	0.2
Space group	$P4_12_12$	$P4_12_12$
a, *b*, *c* (Å)	171.7, 171.7, 99.2	171.7, 171.1, 100.4
Mosaicity (°)	0.15	0.24
Resolution (Å)	49.57–2.50 (2.58–2.50)	48.18–2.80 (2.90–2.80)
Total reflections	710454 (69677)	489576 (49999)
Unique reflections	51712 (5071)	37211 (3643)
Completeness (%)	99.90 (99.90)	99.95 (99.95)
Multiplicity	13.7 (13.7)	13.2 (13.7)
$\langle I/\sigma(I)\rangle$	19.38 (1.44)	15.44 (1.24)
Wilson *B* factor (Å^2)	61.1	76.0
R_{merge}	0.1049 (1.782)	0.1584 (2.240)
R_{meas}	0.109 (1.852)	0.1649 (2.327)
$R_{p.i.m.}$	0.02946 (0.4998)	0.04536 (0.6258)
$CC_{1/2}$	0.999 (0.748)	0.999 (0.512)
CC*	1.00 (0.93)	1.00 (0.82)

rate of the reaction did not permit the determination of steady-state kinetic parameters (Supplementary Fig. S2).

2.4. Dynamic light scattering

Protein samples at 1 mg ml^{-1} in 50 m*M* MOPS pH 7.4, 1 m*M* $MgCl_2$ were centrifuged prior to data collection. Data were collected on a Protein Solutions DynaPro 99 instrument at a wavelength of 8363 Å for 200 s (10 s each for 20 acquisitions) at 25°C. The polydispersity (the standard deviation of the hydrodynamic radius) was 0% for the T337M variant and 30.4% for the G391V variant, which is slightly above the 25% cutoff for a monodisperse sample.

2.5. Circular dichroism

Protein samples (7 m*M*) in 10 m*M* MOPS pH 7.4 were analyzed at 25°C in a 0.5 mm quartz cuvette with a Chirascan V100 spectrometer (Applied Photophysics) equipped with a multi-cell turret and a Peltier temperature-controlled cell holder. Background subtraction was performed using buffer as a reference. For thermal denaturation, samples were heated simultaneously from 5 to 90°C in steps of 5°C while monitoring the ellipticity at 222 nm. Sample aggregation began to occur above a temperature of 65°C, so these data points were not included in the calculation of T_m. As thermal denaturation of PGM1 is not reversible, the apparent T_m reports on both the thermal stability and the kinetics of unfolding in this system.

2.6. 1-Anilino-8-naphthalene sulfonate (ANS) binding

ANS binding assays were performed by incubating 10 m*M* protein with 5.0 m*M* ANS in 50 m*M* MOPS pH 7.4 for 1 h at 25°C as described in Stiers & Beamer (2018*b*). Data were collected using a BioTek Synergy H1 Microplate Reader. The excitation wavelength was 365 nm and emission spectra were recorded from 400 to 560 nm. Relative fluorescence intensities of samples were corrected for ANS emission spectra in buffer. To control for possible effects of phosphorylation of Ser117 on enzyme flexibility, all protein samples were prepared in their dephosphorylated state (Lee *et al.*, 2014).

2.7. X-ray diffraction data collection and refinement

Diffraction data were collected as shown in Table 3 and were processed using *XDS* (Kabsch, 2010) and *AIMLESS* (Evans & Murshudov, 2013) via *CCP*4*i* (Potterton *et al.*, 2003). Data-processing statistics are listed in Table 4. Values of $CC_{1/2}$ > 0.30 (Karplus & Diederichs, 2012) and $R_{p.i.m.}$ (Weiss, 2001) were used to determine the high-resolution cutoff due to the high redundancy obtained with the shutterless data collection.

Structures of the variants were solved by Fourier synthesis. Crystallographic refinement calculations were initiated using the coordinates of WT PGM1 (PDB entry 5epc; Stiers *et al.*, 2016). Refinement was performed with *Phenix* (Liebschner *et*

Table 4
Structure refinement.

Values in parentheses are for the outer shell.

	T337M	G391V
PDB code	7s0w	7s77
No. of reflections, working set	51675 (5069)	37204 (3643)
No. of reflections, test set	2595 (233)	1862 (181)
Final R_{cryst}	0.2140 (0.3060)	0.1927 (0.3162)
Final R_{free}	0.2667 (0.3668)	0.2520 (0.3765)
CC(work)	0.952 (0.830)	0.962 (0.739)
CC(free)	0.920 (0.684)	0.892 (0.534)
No. of non-H atoms		
Total	7910	7916
Protein	7773	7880
Ligands	73	5
Water	64	31
No. of protein residues	1056	1077
R.m.s. deviations		
Bond lengths (Å)	0.008	0.010
Angles (°)	1.23	1.38
Ramachandran plot		
Favored (%)	94.5	94.1
Allowed (%)	4.7	5.1
Outliers (%)	0.8	0.8
Average *B* factor (Å^2)		
Protein	78.0	82.3
Ligands		
Co^{2+}	45.8	—
Sulfate	112.0	148.0
Glycerol	90.1	—
Water	56.2	62.2

al., 2019); progress was monitored by following R_{free}, setting aside 5% of each data set for cross-validation. The *B*-factor model consisted of an isotropic *B* factor for each atom; TLS refinement was used as automated in *Phenix*. *Coot* (Emsley *et al.*, 2010) was used for model building. Structures were validated using *MolProbity* (Chen *et al.*, 2010) and refinement statistics are listed in Table 4. Structural figures were prepared with *PyMOL* (DeLano, 2002). Due to disordered regions in chain *B* of both structures, chain *A* was solely used for figures and structural analyses. Coordinates and structure-factor amplitudes have been deposited in the PDB under the accession codes listed in Table 4.

3. Results

3.1. Impaired enzyme activity of missense variants

The T337M and G391V variant proteins were expressed recombinantly in *E. coli* and purified as described in Section 2 and in Lee *et al.* (2014). Soluble protein was obtained for both variants, although at levels somewhat below that of the WT enzyme (about 50%). Potential aggregation of the purified proteins was assessed by dynamic light scattering. Hydrodynamic radii (R_h) near the expected molecular weight of the monomeric protein were obtained (Table 5).

The variants were also characterized for the competence of their catalytic serine to be phosphorylated by the known activator and reaction intermediate G16P (Table 5). As the PGM1 reaction requires the phosphorylation of an active-site serine (Ser117), the phosphorylation state of this residue provides information on whether it is possible for the enzyme to proceed with catalysis (Lee *et al.*, 2014; Stiers & Beamer, 2018*b*). Using electrospray ionization mass spectrometry, the percentage of the sample modified by phosphorylation in the intact enzyme was assessed before and after treatment with G16P. Both variants show reduced phosphorylation compared with the WT enzyme prior to treatment with G16P (Table 5, Supplementary Fig. S1). In the case of the T337M variant, a significant increase in phosphorylation was found following the addition of the G16P activator, similar to as occurs with the WT enzyme. On the other hand, phosphorylation of the G391V variant increased only slightly, from 0% to just 17%, making it one of the least phosphorylation-competent variants of PGM1 under the conditions tested (Lee *et al.*, 2014).

The kinetic parameters of the T337M variant have previously been characterized (Wong *et al.*, 2015), with a k_{cat}/K_m of ∼2% that of the WT enzyme (data are summarized in Table 5). Impacts on both k_{cat} and K_m are apparent, with the former being the most significant. In the case of the G391V variant, the enzyme activity was too low to permit characterization of the steady-state kinetic parameters (Supplementary Fig. S2). Some phosphoglucomutase activity could be observed over extended times (hours) at very high enzyme concentrations (100-fold that of the WT enzyme). For reference, other PGM1 missense variants with a k_{cat} as low as 0.1% of that of the WT enzyme were still quantifiable (Lee *et al.*, 2014). The near-lack of activity of the G391V variant is consistent with the low levels of phosphorylation of Ser117, which is a prerequisite for enzyme activity.

3.2. Variants show reductions in stability and increased binding of ANS

To probe the effects of the variants on PGM1 stability, we utilized circular dichroism (CD). Apparent melting temperatures (T_m) for the variants were determined via thermal denaturation monitored at 220 nm (Fig. 1*a*). Both variants show a significant reduction in stability, with a T_m approximately 6–7°C below that of the WT enzyme (Table 5). This decrease in stability exceeds that of 1–3°C seen for most other PGM1 missense variants (Lee *et al.*, 2014), except for one remote from the active site that showed a >10°C reduction from the WT (Stiers *et al.*, 2020).

To further probe the effects of the missense mutations on protein conformation, binding of the amphipathic dye 1-anilino-8-naphthalene sulfonate (ANS) was monitored by fluorescence (Fig. 1*b*). ANS binds to nonpolar regions of proteins, including to partially folded and molten-globule-like states (Ray & Balaram, 1999; Hackney & McGoff, 2016), and may serve as a qualitative indication of protein flexibility. We tested three PGM1 variants in comparison with the WT enzyme. At its peak value near 480 nm, the fluorescence of ANS with the T337M variant is slightly below that of the WT enzyme. In contrast, significantly increased fluorescence is observed with the G391V variant. For comparison, another PGM1 missense variant, G291R, was measured in the same experiment. A previous study had shown the G291R variant to

Table 5
Summary of biochemical data on the T337M and G391V PGM1 variants.

n.c., not characterizable. Phosphorylation of Ser117 was assessed via electrospray ionization mass spectrometry as described in Section 2. Apparent molecular weight (MW) and hydrodynamic radius (R_h) were determined by dynamic light scattering. T_m was measured by CD.

Sample	Soluble protein (%)	Apparent MW (kDa)	R_h (nm)	T_m (°C)	k_{cat} (s^{-1})	K_m (μM)	k_{cat}/K_m (μM^{-1} s^{-1})	Phosphorylation before/after G16P (%)
WT†	90	67	3.7	58.2	143 ± 2	80 ± 4	1.8 ± 0.1	35/90
T337M	30	72	3.8	52.2	8.4 ± 0.3‡	206 ± 20‡	0.041 ± 0.004‡	15/91
G391V	80	51	3.3	51.8	n.c.	n.c.	n.c.	0/17

† The data for WT PGM1 have previously been published (Lee *et al.*, 2014). ‡ The kinetic parameters for the T337M variant have previously been published (Wong *et al.*, 2015).

have the greatest contrast with WT PGM1 in ANS binding and other measures of flexibility, including susceptibility to proteolysis (Lee *et al.*, 2014). Fig. 1(*b*) shows that the fluorescence of ANS with G391V is intermediate between those of the WT and the G291R variant, suggesting that a structural perturbation is caused by the mutation, but with somewhat less impact than that of the Gly→Arg substitution at residue 291.

3.3. Structure determination and structural context of the variants

Crystal structures of both the T337M and G391V variants of human PGM1 were determined (Section 2). The proteins crystallized with isomorphous lattices to that of the WT enzyme (Table 3). Two identical copies of the polypeptide chain are found in the asymmetric unit: chain *A* is more highly ordered in all PGM1 crystals and is therefore used as the reference in the following structural descriptions. The resolution of the diffraction data for the two variants was reduced relative to the WT enzyme (1.8 Å) at 2.5 and 2.8 Å for the T337M and G391V variants, respectively. In each structure, the substituted residue (*i.e.* Met or Val) is clearly observed in the electron-density maps.

PGM1 is a four-domain protein with its active site located in a large central cleft (Fig. 2*b*). Both Thr337 and Gly391 are located within domain 3 of PGM1, which spans residues 305–421, and they are also near the interfaces with other domains of the protein (Figs. 2*b*, 3 and 4). T337M is found at the N-terminus of an α-helix and is adjacent to domain 4 of PGM1 (Fig. 3*b*). Its side-chain hydroxyl makes a hydrogen bond to the side-chain hydroxyl of Ser334, and its backbone carbonyl makes a hydrogen bond to the side chain of Arg499 in domain 4. Gly391 is also located at the N-terminus of an α-helix and is positioned directly adjacent to the metal-binding loop in domain 2 of the enzyme (Fig. 4*b*). Its backbone amide makes a hydrogen bond to the backbone carbonyl of Gly291, which is a conserved residue within the critical metal-binding loop of PGM1 (residues 288–292) located in domain 2 of the protein.

3.4. The T337M variant causes a minor shift of a nearby active-site loop

A superposition of the polypeptide backbone of the T337M variant with that of WT PGM1 shows that the structures are very similar (Fig. 3*a*). The overall root-mean-square deviation (r.m.s.d.) between the T337M variant and the WT enzyme is 0.35 Å for 557 C^{α} pairs. Relative to the WT structure, the methionine substitution necessitates the loss of the side-chain hydrogen bond to Ser344, although the backbone interaction

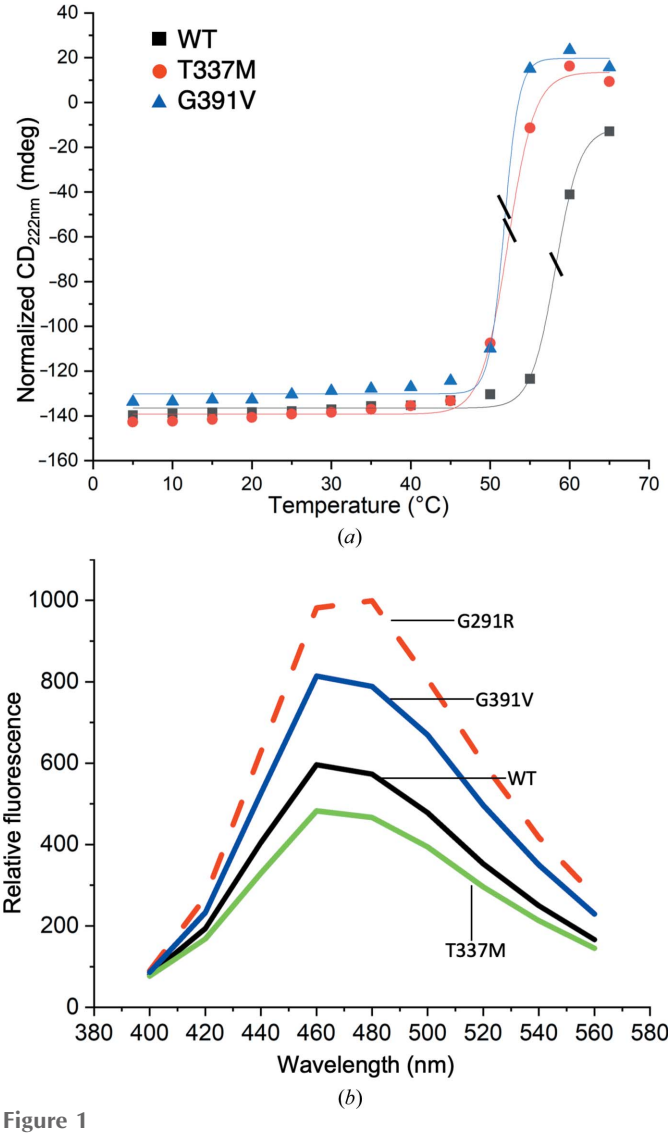

Figure 1
CD and ANS-binding studies of the T337M and G391V variants of PGM1. (*a*) Overlay of melting curves of WT (black), T337M variant (red) and G391V variant (blue) proteins monitored by CD at 222 nm. The midpoint of each curve corresponding to the T_m is indicated by a black bar. (*b*) Binding of ANS to WT PGM1 and to the G291R, T337M and G391V variants monitored by fluorescence (λ_{ex} = 365 nm). The G291R variant of PGM1 was also characterized for comparison as it showed the largest difference from WT PGM1 in a previous study (Lee *et al.*, 2014).

with Arg499 is retained. An alternative view of the structure (Supplementary Fig. S3*a*) highlights the residues in the T337M variant that show the largest displacement from WT PGM1 based on their structural superposition. Except for some surface loops that also show small differences, the major effect of the T337M variant is a small shift of a nearby loop of domain 3 spanning residues 375–381 (Fig. 3*c*). This loop is found in the active-site cleft of PGM1 and contains two conserved ligand-binding residues: Glu376 and Ser378. Both of these residues are implicated in forming interactions with the sugar hydroxyls in enzyme substrate and product complexes (Backe *et al.*, 2020; Stiers & Beamer, 2018*a*; Stiers *et al.*, 2016). Compared with WT PGM1, the C^{α} positions of Glu376 and Ser378 differ by 0.8 and 1.3 Å, respectively. Although small, the shift of this key ligand-binding loop would likely perturb the positioning of the substrate for catalysis and is consistent with the reduced catalytic efficiency (k_{cat}/K_m) observed at ∼2% that of the WT enzyme.

3.5. The G391V variant causes widespread structural perturbation

Unlike the small but impactful structural changes caused by the T337M variant, the G391V mutation produces widespread effects on the PGM1 structure (Fig. 4). A structural superposition yields an overall C^{α} r.m.s.d. of 0.9 Å for 542 C^{α} pairs. Highlighting the displaced residues in the structure of the G391V variant (Supplementary Fig. S3*b*) shows that both the number of residues and the extent of displacement from the WT enzyme are increased compared with the effects observed in the T337M variant. A significant shift (∼5 Å in the backbone) occurs in the metal-binding loop of G391V (Fig. 4*c*), with concomitant loss of the bound metal ion. In addition, the nearby side chains of Trp359 and Phe379 undergo packing rearrangements in the hydrophobic interior of the protein, filling spaces created by the new position of the metal-binding loop (Supplementary Fig. S4).

Beyond the shift of the metal-binding loop, an even greater perturbation in the G391V structure is observed in the active-site loop containing the catalytic phosphoserine, with a 7.4 Å change in the C^{α} position of Ser117 relative to the WT enzyme (Fig. 4*c*). The displacement of the metal-binding and phosphoserine loops has a cascading effect across the structure of domain 1, with additional regions displaced, as evident in Supplementary Fig. S3(*b*). Furthermore, a number of residues in the structure of G391V are not observed in the electron-density map relative to the WT enzyme. In chain *A* these disordered regions include a stretch of nine residues (258–266), as well as three residues following the catalytic phosphoserine (122–124).

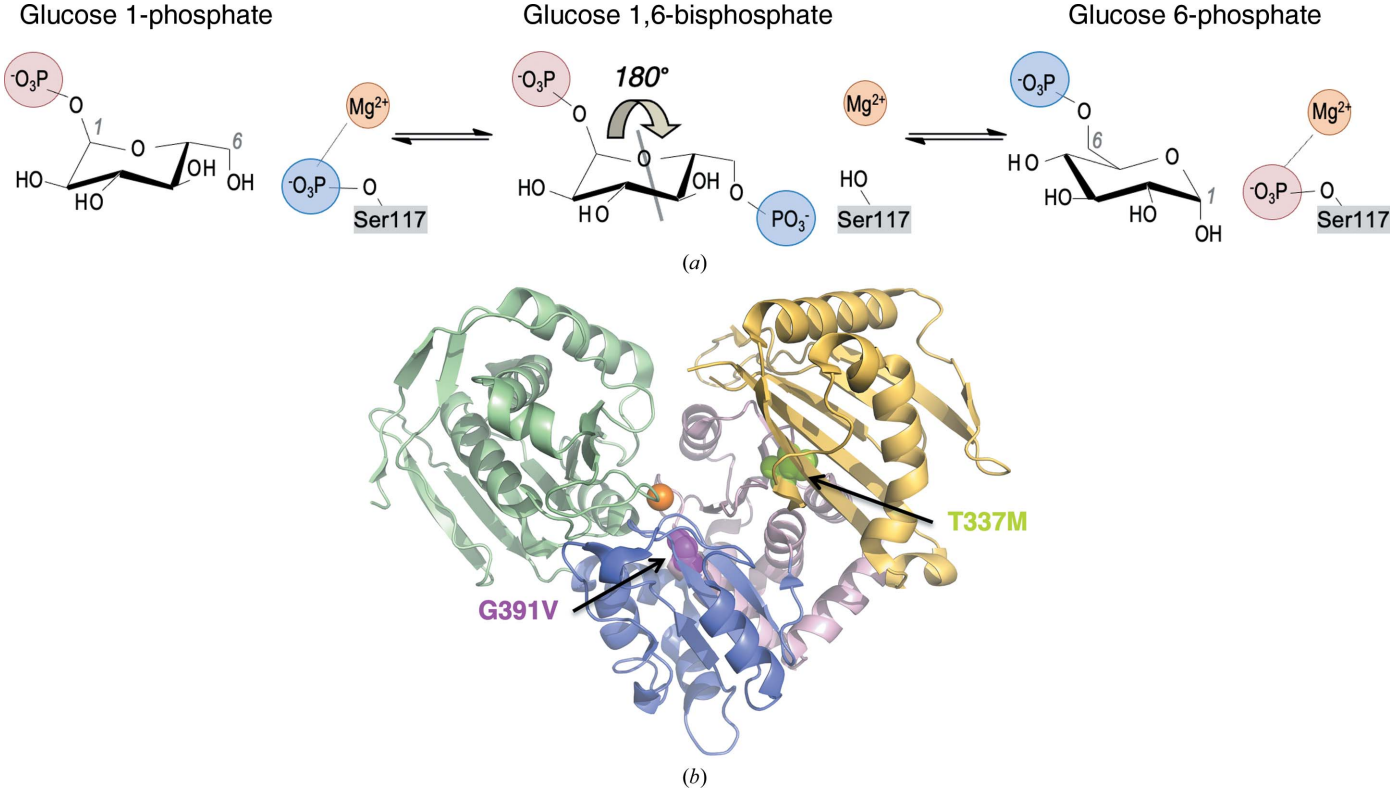

Figure 2
Overview of the mechanism and structure of PGM1. (*a*) The catalytic mechanism of PGM1, showing the reversible conversion of glucose 1-phosphate and glucose 6-phosphate via the G16P bisphosphorylated intermediate. The curved arrow indicates the 180° flip of G16P that occurs between phosphoryl-transfer steps. (*b*) The crystal structure of WT human PGM1 colored according to domain. Domain 1, pale green; domain 2, blue; domain 3, light pink; domain 4, yellow. The catalytic Mg^{2+} ion is shown as an orange sphere. The two residues affected by the disease-related variants described in this study (Thr337 and Gly391) are highlighted.

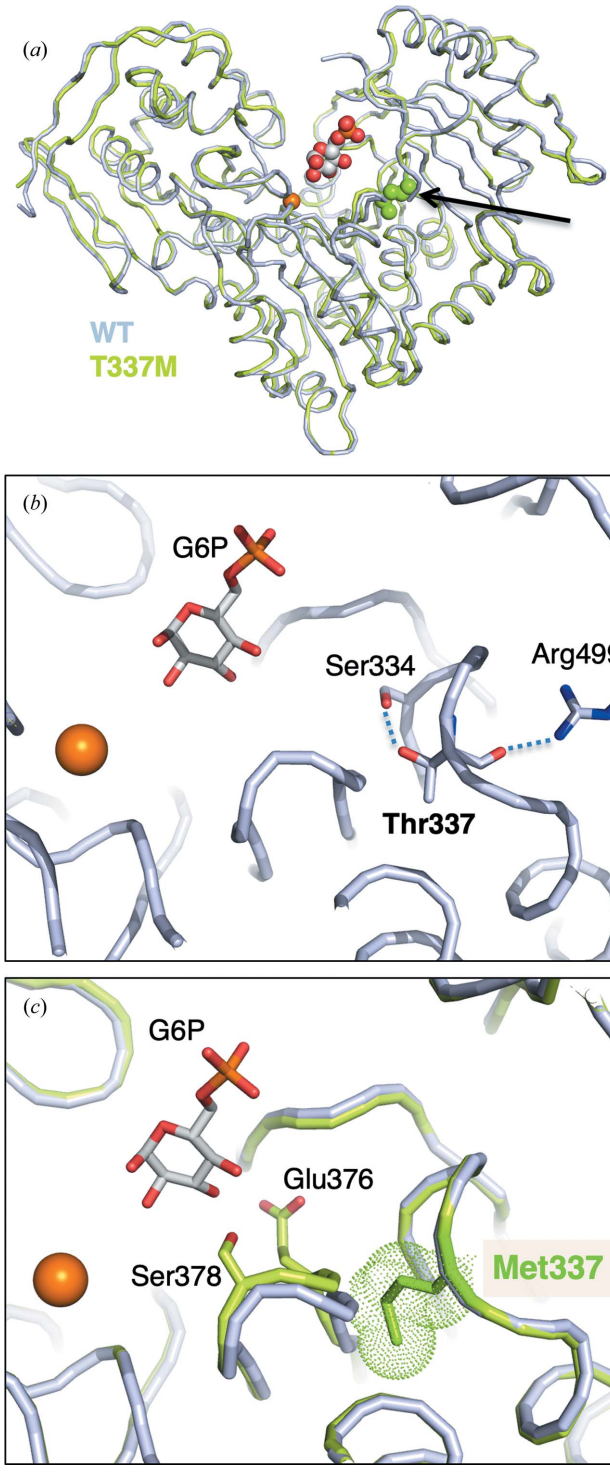

Figure 3
Structural context and effects of the T337M variant in human PGM1. (*a*) A superposition of WT PGM1 (gray) with the T337M variant (green). The metal ion is shown as an orange sphere and Met337 is shown as spheres and highlighted with a black arrow. (*b*) A close-up view of the vicinity of Thr337 in WT PGM1 (PDB entry 5epc). Dashed lines indicate hydrogen bonds. The substrate glucose 6-phosphate is shown as bound in the active site of PDB entry 6bj0 (Stiers & Beamer, 2018*a*). (*c*) A close-up view of the vicinity of the T337M variant superposed with WT PGM1. Colors are as in (*a*). The side chains of two key ligand-binding residues, Glu376 and Ser378, are shown as sticks. The small shift in the backbone of the loop containing these residues can be seen in comparison with the WT enzyme.

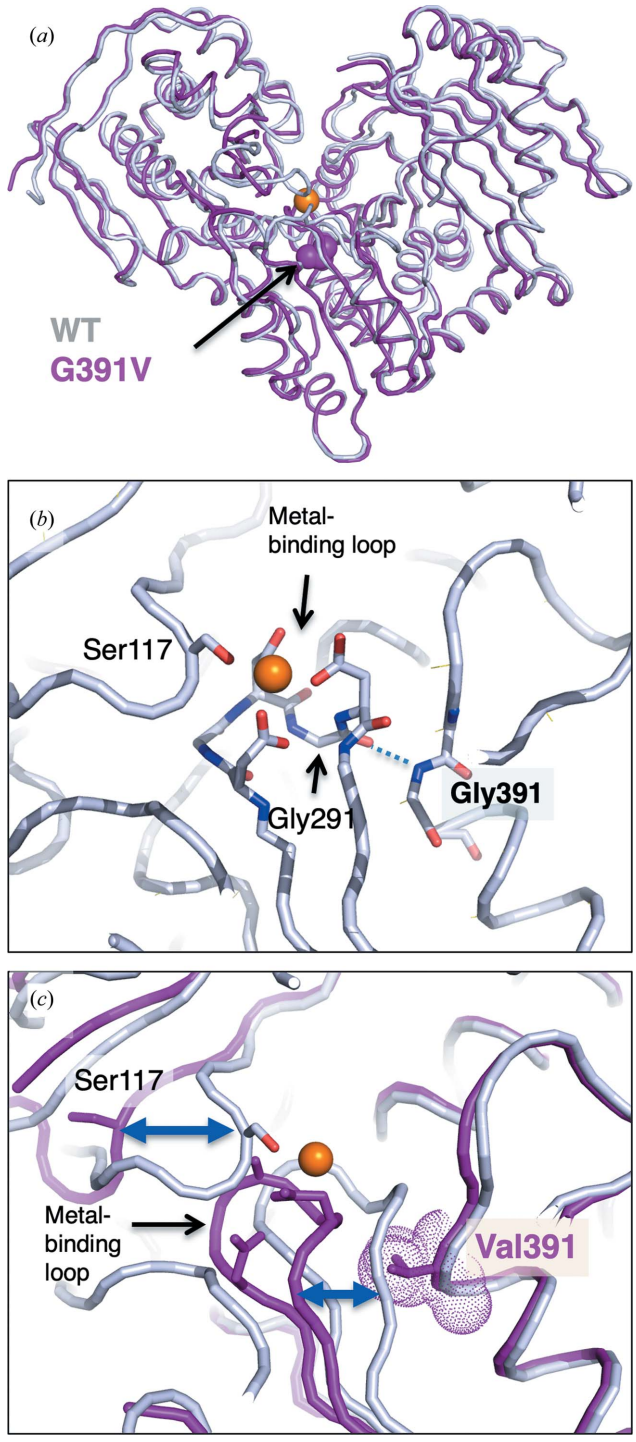

Figure 4
Structural context and effects of the G391V variant in human PGM1. (*a*) A superposition of WT PGM1 (gray) with the G391V variant (magenta). The metal ion is shown as an orange sphere and Gly391 is shown as spheres and highlighted with a black arrow. (*b*) A close-up view of the vicinity of Gly391 in WT PGM1 (PDB entry 5epc). The dashed line indicates a hydrogen bond. Gly391 and residues in the metal-binding loop are shown in stick representation. (*c*) A close-up view of the vicinity of the G391V variant superposed with WT PGM1. Colors are as in (*a*). Large shifts in the backbone of the loops containing the catalytic phosphoserine (Ser117) and metal-binding residues are seen in comparison with the WT enzyme and are highlighted with blue arrows. The metal ion in this panel is from WT enzyme; no bound metal ion is seen in the G391V variant (see text).

The widespread structural effects of the G391V variant are noteworthy given that the valine substitution results in the introduction of only a few extra non-H atoms in the 562-residue enzyme. However, the location of the variant, directly adjacent to the conserved metal-binding loop, explains the observed structural impacts, as well as the greatly impaired enzyme activity and low level of phosphorylation of Ser117. The structural perturbation spanning multiple domains (Supplementary Fig. S3*b*) also correlates with increased fluorescence of ANS, suggesting increased access of the dye to hydrophobic binding sites. Although the G391V protein crystallizes and might therefore be considered to be well folded, the diffraction resolution of the X-ray data is significantly lower than that of the WT (2.8 versus 1.8 Å), which could reflect increased structural heterogeneity within the crystal of the G391V mutant. It is perhaps also worth noting that the X-ray diffraction data were collected at a very low temperature (100 K) and that the protein structure could be considerably more flexible/disordered at room temperature (Fraser *et al.*, 2011).

4. Conclusions

The two PGM1 variants characterized here show large contrasts in their structural impacts despite their generally similar effects on enzyme function. A common feature of both variants is their location near interdomain interfaces of the protein and their proximity to key active-site loops. In both cases, the structural context appears to outweigh what might be expected based on the physicochemical change of the substitution. For example, the Thr→Met substitution is a change to a larger side chain as well as a more hydrophobic one. While increased size could cause structural clashes, the hydrophobicity of the methionine side chain might also contribute to increased stability by packing in the protein interior. Our data show that the small but detrimental steric change has the predominant effect on the enzyme function of the T337M variant due to a shift of the active-site loop. In the case of the G391V variant, the Gly→Val substitution also has the potential to produce steric clashes, although this might only be significant in a tightly packed environment, which is indeed the case here. As noted above, although the valine side chain is rather small, a cascade of structural rearrangements occur, spanning three of the four domains of the enzyme and producing an essentially inactive enzyme.

A preponderance of PGM1-CDG variants located near interdomain interfaces has previously been noted, an observation that is likely to be correlated with the location of the enzyme active site at the confluence of its four structural domains (Stiers *et al.*, 2016). Several other variants in this category have widespread impacts similar to those of G391V, including G121R and G291R. The crystal structures of these two variants show similarities, including the introduction of disordered regions of the polypeptide, a loss of metal binding in the G291R variant, a decreased diffraction resolution and packing differences in the hydrophobic core (Stiers *et al.*, 2016). Notably, both of these variants have a dramatic physicochemical change (Gly→Arg) and are also *within* key active-site loops, not simply adjacent as is the case for the G391V variant. Nonetheless, the extent of the structural perturbation in the G391V variant appears to approach that of the G291R variant based on structural comparisons and ANS-binding data. These results emphasize the complexity of trying to elucidate the molecular pathomechanisms of missense variants, even when both sequence and structural information are available.

The T337M and G391V variant proteins characterized here represent the tenth and eleventh crystal structures of PGM1-CDG missense variants to be determined (Stiers *et al.*, 2016, 2020; Stiers, Graham *et al.*, 2017; Stiers & Beamer, 2018*a*). Through its ability to accommodate significant perturbation, the robust, multi-domain structure of the enzyme has enabled detailed structural characterization of its variants, making this system a paradigm for understanding the molecular impacts of mutations related to inherited metabolic disease (Beamer, 2021). Insights from studies of PGM1 have potential implications for related proteins, including two paralogs, PGM2L1 and PGM3, found in the human genome (Muenks *et al.*, 2017). Both of these proteins belong to the same α-D-phosphohexomutase enzyme superfamily as PGM1 (Stiers, Muenks *et al.*, 2017) and have recently been identified to be associated with inherited enzyme deficiencies (Fusaro *et al.*, 2021; Liu *et al.*, 2020; Lundin *et al.*, 2015; Ben-Khemis *et al.*, 2017; Sassi *et al.*, 2014; Zhang *et al.*, 2014; Stray-Pedersen *et al.*, 2014; Morava *et al.*, 2021). Due to similar protein architectures and highly conserved active-site regions, the molecular pathomechanisms elucidated in PGM1 variants may also be relevant in these related systems.

Acknowledgements

We thank Brian Mooney of the University of Missouri Charles W. Gehrke Proteomics Center for mass spectrometry, Mike Henzl for useful discussions about circular dichroism and Jay Nix of Advanced Light Source (ALS) beamline 4.2.2 for assistance with data collection and processing. Part of this work was performed at the ALS, which is supported by the Director, Office of Science, Office of Basic Energy Sciences of the US Department of Energy under contract DE-AC02-05CH11231. Other research reported in this publication was supported by the Office Of The Director, National Institutes Of Health under Award No. S10OD026703. The content is solely the responsibility of the authors and does not necessarily represent the official views of the National Institutes of Health.

Funding information

Funding for this project was provided in part by a TRIUMPH award to LJB from the University of Missouri School of Medicine.

References

Altassan, R., Radenkovic, S., Edmondson, A. C., Barone, R., Brasil, S., Cechova, A., Coman, D., Donoghue, S., Falkenstein, K., Ferreira,

V., Ferreira, C., Fiumara, A., Francisco, R., Freeze, H., Grunewald, S., Honzik, T., Jaeken, J., Krasnewich, D., Lam, C., Lee, J., Lefeber, D., Marques-da-Silva, D., Pascoal, C., Quelhas, D., Raymond, K. M., Rymen, D., Seroczynska, M., Serrano, M., Sykut-Cegielska, J., Thiel, C., Tort, F., Vals, M. A., Videira, P., Voermans, N., Witters, P. & Morava, E. (2021). *J. Inherit. Metab. Dis.* **44**, 148–163.

Backe, P. H., Laerdahl, J. K., Kittelsen, L. S., Dalhus, B., Mørkrid, L. & Bjørås, M. (2020). *Sci. Rep.* **10**, 5656.

Beamer, L. J. (2021). *Biochimie*, **183**, 44–48.

Ben-Khemis, L., Mekki, N., Ben-Mustapha, I., Rouault, K., Mellouli, F., Khemiri, M., Bejaoui, M., Essaddam, L., Ben-Becher, S., Boughamoura, L., Hassayoun, S., Ben-Ali, M. & Barbouche, M.-R. (2017). *Mol. Immunol.* **90**, 57–63.

Chen, V. B., Arendall, W. B., Headd, J. J., Keedy, D. A., Immormino, R. M., Kapral, G. J., Murray, L. W., Richardson, J. S. & Richardson, D. C. (2010). *Acta Cryst.* D**66**, 12–21.

DeLano, W. L. (2002). *PyMOL.* http://www.pymol.org.

Ding, Y., Li, N., Chang, G., Li, J., Yao, R., Shen, Y., Wang, J., Huang, X. & Wang, X. (2018). *J. Pediatr. Endocrinol. Metab.* **31**, 781–788.

Donoghue, S. E., White, S. M., Tan, T. Y., Kowalski, R., Morava, E. & Yaplito-Lee, J. (2021). *JIMD Rep.* **57**, 29–37.

Emsley, P., Lohkamp, B., Scott, W. G. & Cowtan, K. (2010). *Acta Cryst.* D**66**, 486–501.

Evans, P. R. & Murshudov, G. N. (2013). *Acta Cryst.* D**69**, 1204–1214.

Fraser, J. S., van den Bedem, H., Samelson, A. J., Lang, P. T., Holton, J. M., Echols, N. & Alber, T. (2011). *Proc. Natl Acad. Sci. USA*, **108**, 16247–16252.

Fusaro, M., Vincent, A., Castelle, M., Rosain, J., Fournier, B., Veiga-da-Cunha, M., Kentache, T., Serre, J., Fallet-Bianco, C., Delezoide, A. L., Renesme, L., Picard, F. M., Lasseaux, E., Aladjidi, N., Seta, N., Cormier-Daire, V., Schaftingen, E. V., Neven, B., Moshous, D., Blesson, S. & Picard, C. (2021). *J. Clin. Immunol.* **41**, 958–966.

Hackney, D. D. & McGoff, M. S. (2016). *Arch. Biochem. Biophys.* **608**, 42–51.

Kabsch, W. (2010). *Acta Cryst.* D**66**, 125–132.

Karplus, P. A. & Diederichs, K. (2012). *Science*, **336**, 1030–1033.

Küçükçongar, A., Tümer, L., Ezgü, F. S., Kasapkara, Ç. S., Jaeken, J., Matthijs, G., Rymen, D., Dalgiç, B., Bıdecı, A. & Hasanoğlu, A. (2015). *Genet. Couns.* **26**, 87–90.

Lee, Y., Stiers, K. M., Kain, B. N. & Beamer, L. J. (2014). *J. Biol. Chem.* **289**, 32010–32019.

Liebschner, D., Afonine, P. V., Baker, M. L., Bunkóczi, G., Chen, V. B., Croll, T. I., Hintze, B., Hung, L.-W., Jain, S., McCoy, A. J., Moriarty, N. W., Oeffner, R. D., Poon, B. K., Prisant, M. G., Read, R. J., Richardson, J. S., Richardson, D. C., Sammito, M. D., Sobolev, O. V., Stockwell, D. H., Terwilliger, T. C., Urzhumtsev, A. G., Videau, L. L., Williams, C. J. & Adams, P. D. (2019). *Acta Cryst.* D**75**, 861–877.

Liu, X.-R., Bian, W.-J., Wang, J., Ye, T.-T., Li, B.-M., Liu, D.-T., Tang, B., Deng, W.-W., Shi, Y.-W., Su, T., Yi, Y.-H. & Liao, W.-P. (2020). *Front. Genet.* **11**, 559080.

Lundin, K. E., Hamasy, A., Backe, P. H., Moens, L. N., Falk-Sörqvist, E., Elgstøen, K. B., Mørkrid, L., Bjørås, M., Granert, C., Norlin, A. C., Nilsson, M., Christensson, B., Stenmark, S. & Smith, C. I. E. (2015). *Clin. Immunol.* **161**, 366–372.

Morava, E., Schatz, U. A., Torring, P. M., Abbott, M., Baumann, M., Brasch-Andersen, C., Chevalier, N., Dunkhase-Heinl, U., Fleger, M., Haack, T. B., Nelson, S., Potelle, S., Radenkovic, S., Bommer, G. T., Van Schaftingen, E. & Veiga-da-Cunha, M. (2021). *Am. J. Hum. Genet.* **108**, 1151–1160.

Morava, E., Wong, S. & Lefeber, D. (2015). *J. Inherit. Metab. Dis.* **38**, 207–209.

Muenks, A. G., Stiers, K. M. & Beamer, L. J. (2017). *PLoS One*, **12**, e0183563.

Nolting, K., Park, J. H., Tegtmeyer, L. C., Zühlsdorf, A., Grüneberg, M., Rust, S., Reunert, J., Du Chesne, I., Debus, V., Schulze-Bahr, E., Baxter, R. C., Wada, Y., Thiel, C., van Schaftingen, E., Fingerhut, R. & Marquardt, T. (2017). *Mol. Genet. Metab. Rep.* **13**, 33–40.

Ondruskova, N., Honzik, T., Vondrackova, A., Tesarova, M., Zeman, J. & Hansikova, H. (2014). *Neuro Endocrinol. Lett.* **35**, 137–141.

Pérez, B., Medrano, C., Ecay, M. J., Ruiz-Sala, P., Martínez-Pardo, M., Ugarte, M. & Pérez-Cerdá, C. (2013). *J. Inherit. Metab. Dis.* **36**, 535–542.

Potterton, E., Briggs, P., Turkenburg, M. & Dodson, E. (2003). *Acta Cryst.* D**59**, 1131–1137.

Quick, C. B., Fisher, R. A. & Harris, H. (1974). *Eur. J. Biochem.* **42**, 511–517.

Radenkovic, S., Bird, M. J., Emmerzaal, T. L., Wong, S. Y., Felgueira, C., Stiers, K. M., Sabbagh, L., Himmelreich, N., Poschet, G., Windmolders, P., Verheijen, J., Witters, P., Altassan, R., Honzik, T., Eminoglu, T. F., James, P. M., Edmondson, A. C., Hertecant, J., Kozicz, T., Thiel, C., Vermeersch, P., Cassiman, D., Beamer, L., Morava, E. & Ghesquière, B. (2019). *Am. J. Hum. Genet.* **104**, 835–846.

Ray, S. S. & Balaram, P. (1999). *J. Phys. Chem. B*, **103**, 7068–7072.

Sassi, A., Lazaroski, S., Wu, G., Haslam, S. M., Fliegauf, M., Mellouli, F., Patiroglu, T., Unal, E., Ozdemir, M. A., Jouhadi, Z., Khadir, K., Ben-Khemis, L., Ben-Ali, M., Ben-Mustapha, I., Borchani, L., Pfeifer, D., Jakob, T., Khemiri, M., Asplund, A. C., Gustafsson, M. O., Lundin, K. E., Falk-Sörqvist, E., Moens, L. N., Gungor, H. E., Engelhardt, K. R., Dziadzio, M., Stauss, H., Fleckenstein, B., Meier, R., Prayitno, K., Maul-Pavicic, A., Schaffer, S., Rakhmanov, M., Henneke, P., Kraus, H., Eibel, H., Kölsch, U., Nadifi, S., Nilsson, M., Bejaoui, M., Schäffer, A. A., Smith, C. I. E., Dell, A., Barbouche, M. & Grimbacher, B. (2014). *J. Allergy Clin. Immunol.* **133**, 1410–1419.

Schjoldager, K. T., Narimatsu, Y., Joshi, H. J. & Clausen, H. (2020). *Nat. Rev. Mol. Cell Biol.* **21**, 729–749.

Stiers, K. M. & Beamer, L. J. (2018*a*). *Structure*, **26**, 1337–1345.

Stiers, K. M. & Beamer, L. J. (2018*b*). *Methods Enzymol.* **607**, 241–267.

Stiers, K. M., Graham, A. C., Kain, B. N. & Beamer, L. J. (2017). *FEBS J.* **284**, 937–947.

Stiers, K. M., Hansen, R. P., Daghlas, B. A., Mason, K. N., Zhu, J.-S., Jakeman, D. L. & Beamer, L. J. (2020). *J. Inherit. Metab. Dis.* **43**, 861–870.

Stiers, K. M., Kain, B. N., Graham, A. C. & Beamer, L. J. (2016). *J. Mol. Biol.* **428**, 1493–1505.

Stiers, K. M., Muenks, A. G. & Beamer, L. J. (2017). *Adv. Protein Chem. Struct. Biol.* **109**, 265–304.

Stojkovic, T., Vissing, J., Petit, F., Piraud, M., Orngreen, M. C., Andersen, G., Claeys, K. G., Wary, C., Hogrel, J.-Y. & Laforêt, P. (2009). *N. Engl. J. Med.* **361**, 425–427.

Stray-Pedersen, A., Backe, P. H., Sorte, H. S., Mørkrid, L., Chokshi, N. Y., Erichsen, H. C., Gambin, T., Elgstøen, K. B. P., Bjørås, M., Wlodarski, M. W., Krüger, M., Jhangiani, S. N., Muzny, D. M., Patel, A., Raymond, K. M., Sasa, G. S., Krance, R., Martinez, C. A., Abraham, S. M., Speckmann, C., Ehl, S., Hall, P., Forbes, L. R., Merckoll, E., Westvik, J., Nishimura, G., Rustad, C. F., Abrahamsen, T. G., Rønnestad, A., Osnes, L. T., Egeland, T., Rødningen, O. K., Beck, C. R., Baylor-Johns Hopkins Center for Mendelian Genomics, Boerwinkle, E. A., Gibbs, R. A., Lupski, J. R., Orange, J. S., Lausch, E. & Hanson, I. C. (2014). *Am. J. Hum. Genet.* **95**, 96–107.

Tegtmeyer, L. C., Rust, S., van Scherpenzeel, M., Ng, B. G., Losfeld, M.-E., Timal, S., Raymond, K., He, P., Ichikawa, M., Veltman, J., Huijben, K., Shin, Y. S., Sharma, V., Adamowicz, M., Lammens, M., Reunert, J., Witten, A., Schrapers, E., Matthijs, G., Jaeken, J., Rymen, D., Stojkovic, T., Laforêt, P., Petit, F., Aumaître, O., Czarnowska, E., Piraud, M., Podskarbi, T., Stanley, C. A., Matalon, R., Burda, P., Seyyedi, S., Debus, V., Socha, P., Sykut-Cegielska, J., van Spronsen, F., de Meirleir, L., Vajro, P., DeClue, T., Ficicioglu, C., Wada, Y., Wevers, R. A., Vanderschaeghe, D., Callewaert, N., Fingerhut, R., van Schaftingen, E., Freeze, H. H., Morava, E.,

Lefeber, D. J. & Marquardt, T. (2014). *N. Engl. J. Med.* **370**, 533–542.
Timal, S., Hoischen, A., Lehle, L., Adamowicz, M., Huijben, K., Sykut-Cegielska, J., Paprocka, J., Jamroz, E., van Spronsen, F. J., Körner, C., Gilissen, C., Rodenburg, R. J., Eidhof, I., Van den Heuvel, L., Thiel, C., Wevers, R. A., Morava, E., Veltman, J. & Lefeber, D. J. (2012). *Hum. Mol. Genet.* **21**, 4151–4161.
Weiss, M. S. (2001). *J. Appl. Cryst.* **34**, 130–135.
Wong, S. Y.-W., Beamer, L. J., Gadomski, T., Honzik, T., Mohamed, M., Wortmann, S. B., Brocke Holmefjord, K. S., Mork, M., Bowling, F., Sykut-Cegielska, J., Koch, D., Ackermann, A., Stanley, C. A., Rymen, D., Zeharia, A., Al-Sayed, M., Marquardt, T., Jaeken, J., Lefeber, D., Conrad, D. F., Kozicz, T. & Morava, E. (2015). *J. Pediatr.* **175**, 130–136.
Zeevaert, R., Scalais, E., Muino Mosquera, L., De Meirleir, L., De Beaufort, C., Witsch, M., Jaeken, J. & De Schepper, J. (2016). *Acta Clin. Belg.* **71**, 435–437.
Zhang, Y., Yu, X., Ichikawa, M., Lyons, J. J., Datta, S., Lamborn, I. T., Jing, H., Kim, E. S., Biancalana, M., Wolfe, L. A., DiMaggio, T., Matthews, H. F., Kranick, S. M., Stone, K. D., Holland, S. M., Reich, D. S., Hughes, J. D., Mehmet, H., McElwee, J., Freeman, A. F., Freeze, H. H., Su, H. C. & Milner, J. D. (2014). *J. Allergy Clin. Immunol.* **133**, 1400–1409.